buildings

MDPI

Article

Numerical Study of Micro-Thermal Environment in Block Based on Porous Media Model

Jie Lei [1], Dengyun Wang [2] and Zhenqian Chen [1,3,*]

[1] School of Energy and Environment, Southeast University, Nanjing 210016, China; 220190424@seu.edu.cn
[2] School of Architecture, Southeast University, Nanjing 210016, China; wangdengyunseu@163.com
[3] Jiangsu Provincial Key Laboratory of Solar Energy Science and Technology, Southeast University, Nanjing 210016, China
* Correspondence: zqchen@seu.edu.cn; Tel.: +86-137-7083-8011

Abstract: The mitigation of the heat island effect has become one of the most challenging issues with the rapid urbanization and increased human activities. A standard model and a porous media model were developed to simulate the microthermal environment in the presence of anthropogenic heat in Nanjing Xinjiekou block. The accuracy of the simulation results was verified by field measurement data. Compared with the standard CFD method, the porous media method reduces the number of meshes by 27.8% and the total computation time by 66.7%. By comparing and analyzing the thermal environment of the block with various porosities and heat intensities at different heights, calculations proved that the velocity is positively correlated with the porosity change, and the temperature is negatively correlated with it in contrast. The temperature increases linearly with the increase in anthropogenic heat intensity under the block height range, and the gradient is about 0.025 K/W at the height of 2 m. The porous media approach allows for effective prediction of the micro-thermal environment in the initial stages of urban design while increasing the porosity of the block and controlling the intensity of anthropogenic heat emissions can be a prominent means of improving the thermal environment.

Keywords: micro-thermal environment; porous media; porosity; anthropogenic heat

Citation: Lei, J.; Wang, D.; Chen, Z. Numerical Study of Micro-Thermal Environment in Block Based on Porous Media Model. *Buildings* **2022**, *12*, 595. https://doi.org/10.3390/buildings12050595

Academic Editors: Xingxing Zhang, Mengjie Han and Pei Huang

Received: 7 April 2022
Accepted: 2 May 2022
Published: 4 May 2022

1. Introduction

With the increasing process of urbanization in China, the phenomenon of the urban heat island becomes a serious problem due to the growing total number of buildings and human activities [1]. Computational Fluid Dynamics (CFD) simulation can accurately simulate heat transfer and diffusion in a block [2]; thus, providing the theoretical basis and reference for layout design and planning. Standard CFD simulation requires establishment of a detailed geometric model of the simulation area in large-scale simulations, which is not only complicated for modeling and pre-processing, but also has a long running time, a large amount of calculation, and a corresponding increase in simulation cost [3]. The porous media model can use key parameters to reflect the overall characteristics of the region, simplify the model, and save the amount of calculation [4,5]. Therefore, based on the similarity between building blocks and porous media, a new method for simplifying building groups into porous media has emerged. In 1997, Antohe [6] developed a porous turbulence model to study the flow of porous urban canopy, indicating that the porous media model has certain practical value in simulating large-scale urban areas. Hang [7] regarded the city as a porous media, and the air in the city as an incompressible fluid passing through the porous media. By dividing the whole mixed region into porous urban areas and fluid areas, it is found that this method can significantly reduce the workload of modeling, meshing, and calculation in simulation. Gu Zhaolin et al. [8] used the porous method and experiments to analyze the real urban area and found that the simulation results were in perfect agreement with the wind tunnel experimental results

and verified the validity of the numerical model with the wind tunnel experimental results. Wang et al. [9] compared and analyzed the three simulation results of the actual model, the roughness height model, and the mixed model of porous media modeling in some areas of the building clusters, and found that the porous media model is more effective and accurate than the roughness height model, and requires much less calculation. Li et al. [10] validated the porous media simulation method and micro-scale CFD simulations for a relatively regular arrangement of settlements with a horizontal length of about 1 km in Xi'an, and the results showed that the wind velocity distribution and temperature distribution trends of both were in excellent agreement. Ming et al. [11] established a concentric city structure and obtained the temperature and flow fields over the city using porous media simulations, and analyzed the effects of anthropogenic heat, ambient wind velocity, and porosity in the central region on urban turbulence and heat transfer. It is found that the three-dimensional turbulent porous media model is suitable for estimating the UHI effect. These studies demonstrate the practical value of applying the porous media model to urban building clusters and provide a reference and theoretical basis for this study.

In recent years, researchers have found that anthropogenic heat affects the urban thermal environment at different time and space levels [12], which is one of the main driving forces that exacerbate global warming [13–16]. Especially in the city center area with high building density, the heat dissipation capacity is not ideal due to poor ventilation, and the impact of anthropogenic heat removal on the urban heat island effect cannot be ignored [17,18]. Anthropogenic heat emissions are mainly in the form of industrial heat emissions, traffic heat emissions, and household heat emissions into the atmospheric thermal environment [19,20]. The research on a large amount of urban anthropogenic heat by Du et al. [21] showed that anthropogenic heat played an obvious role in aggravating the urban heat island effect. Xie Min et al. [22] found that anthropogenic heat emissions have apparent regional characteristics, and the anthropogenic heat emissions in areas with a high degree of urbanization are significantly higher than those in other areas. Additionally, anthropogenic heat emissions vary with season and time [23]. Takane et al. [24] explored the impact of the feedback relationship between urban warming and air-conditioning use on atmospheric temperature in future urban climates and found that anthropogenic heat emissions from air-conditioning use would lead to a linear increase in the rate of temperature change. Ohashi et al. [25] found that the waste heat from air conditioners in Osaka City in summer may cause the air temperature to increase by 0.36~0.72 °C. Tong Hua [26] explored the effect of anthropogenic heat on the increase in urban temperature by estimating the intensity of anthropogenic heat emissions in Beijing, and evaluated the effect of reducing anthropogenic heat emissions on mitigating urban heat islands. Jiang Weimei [27] found that the anthropogenic heat sources in Nanjing and Hangzhou could increase the heat island intensity by 1~3 °C. However, the research on anthropogenic heat mostly focuses on the statistical analysis of different anthropogenic heat source intensity in cities in different regions, as well as the analysis of the impact of anthropogenic heat on the thermal environment on the urban and even global scale [28–30]. There is still a lack of research on the use of numerical simulation from the perspective of small and medium scales.

The simulation of predicted airflow around buildings has an essential impact on the outdoor microthermal environment, and the considerable simulation costs are one of the bottlenecks limiting the development of microclimates. There are significant difficulties in using ordinary computers to quickly implement thermal environment calculations in urban spaces, while porous media simulations can provide significant savings in computational costs and computational effort. Research on porous media for urban microthermal environments is still preliminary, and scholars are currently experimenting mainly on ideal building blocks and using wind tunnel experiments for verification. In this paper, an actual block is selected, and measured data are used to verify the applicability of the porous media model in the study of microthermal environments in the actual block. The effect of porosity and anthropogenic heat emissions on the microthermal environment is also explored, considering the inescapable role of anthropogenic heat emissions on the

microthermal environment. The modeling results could be used to guide development of scientific urban development plans to mitigate the UHI effect.

2. Models and Methods

2.1. Macroscopic Turbulence Model

Based on Antohe's [6] derivation, Hang and Li [7] provided a single domain method in the transport equations of the macroscopic k–ε porous model to simulate the idealized building cluster. This approach performed reasonably well in predicting the reduction in flow velocity through the building cluster. The transport equations of the incompressible flow in the urban canopy are as follows.

Continuity equation:

$$\frac{\partial(\rho\phi {u_i}^f)}{\partial x_i} = 0 \tag{1}$$

The momentum conservation equation:

$$\begin{aligned}\frac{\partial(\rho\phi {u_i}^f {u_j}^f)}{\partial x_j} &= \frac{\partial}{\partial x_j}[(\mu_l J_1 + \mu_t)\frac{\partial(\phi {u_i}^f)}{\partial x_j}] - (\frac{\partial(\phi p^f)}{\partial x_i} + \frac{2}{3}\rho\frac{\partial(\phi k^f)}{\partial x_i}) \\ &-\phi^2\frac{\mu}{K}{u_i}^f - \phi^3\rho\frac{C_F}{\sqrt{K}}Q^f {u_i}^f + \delta_{i3}\rho[\beta(T - T_{in}) - 1]\end{aligned} \tag{2}$$

Equation for the turbulent kinetic energy (THK):

$$\begin{aligned}\frac{\partial(\rho\phi {u_i}^f k^f)}{\partial x_j} &= \frac{\partial}{\partial x_j}[(\mu_l J_1 + \frac{\mu_t}{\sigma_k})\frac{\partial(\phi k^f)}{\partial x_j}] - \rho\phi\varepsilon^f + \phi G_k \\ &-2\phi^2\frac{\mu_l}{K}k^f - \frac{8}{3}\phi^3\rho\frac{C_F}{\sqrt{K}}Q^f k^f + 2\phi^3\frac{C_F}{\sqrt{K}}F_k\end{aligned} \tag{3}$$

Equation for the energy dissipation:

$$\begin{aligned}\frac{\partial(\rho\phi {u_i}^f \varepsilon^f)}{\partial x_j} &= \frac{\partial}{\partial x_j}\left[\left(\mu_l J_1 + \frac{\mu_t}{\sigma_\varepsilon}\right)\frac{\partial(\phi\varepsilon^f)}{\partial x_j}\right] - C_{\varepsilon 1}\phi\frac{\varepsilon^f}{k^f}G_k - J_1\rho C_{\varepsilon 2}\phi\frac{\varepsilon^f}{k^f}\varepsilon^f - 2\phi^2\frac{\mu_l}{K}\varepsilon^f - \frac{8}{3}\phi^3\rho\frac{C_F}{\sqrt{K}}Q^f\varepsilon^f \\ &-\frac{8\mu_l}{3}\phi^3\frac{C_F}{\sqrt{K}}\frac{\partial k^f}{\partial x_r}\frac{\partial Q^f}{\partial x_r} + 2\phi^3\frac{C_F}{\sqrt{K}}\left[\mu_l v_t\frac{\partial}{\partial x_r}\left(\frac{{u_i}^f {u_j}^f}{Q^f}\right)\frac{\partial^2 {u_i}^f}{\partial x_r \partial x_j} + 2\mu_l v_t\frac{{u_i}^f {u_j}^f}{Q^f}\frac{\partial^2}{\partial {x_r}^2}\left(\frac{\partial {u_i}^f}{\partial x_j}\right)\right]\end{aligned} \tag{4}$$

where

$$Q^f = \sqrt{{u_i}^f {u_j}^f} \tag{5}$$

$$\mu_t = C_\mu\rho\frac{(k^f)^2}{\varepsilon^f} \tag{6}$$

$$F_k = \mu_t\frac{{u_i}^f {u_j}^f}{Q^f}(\frac{\partial\phi {u_j}^f}{\partial x_i}) \tag{7}$$

$$G_k = \mu_t\frac{\partial {u_i}^f}{\partial x_j}(\frac{\partial {u_i}^f}{\partial x_j} + \frac{\partial {u_j}^f}{\partial x_i}) \tag{8}$$

where ρ is density, ${u_i}^f$, Q^f, p^f, k^f, and ε^f are intrinsic averages of time-averaged velocity components, representing the velocity, pressure turbulence kinetic energy and its dissipation rate, respectively. μ_l and μ_t are the dynamic and turbulent viscosities. J_1 is the viscosity ratio which can be assumed to be 1 for most applications in porous media. σ_k and σ_ε are constant, and the default values are 1.0 and 1.3, respectively.

2.2. Parameterization of Buildings as Porous Media

The porosity is the percentage of pores in the porous media, and the calculation is as follows:

$$\phi = \frac{U_v}{U} = \frac{U - U_s}{U} \tag{9}$$

where ϕ is the porosity, U is the volume of the porous media, U_v is the pore volume of the porous media, and U_s is the volume of the skeleton of the porous media.

On the basis of on-site investigation, the block was divided into 7 building blocks, as shown in Figure 1. Block zone porosity can be determined by calculating the following:

$$\phi = \frac{V - \sum V_i}{V} = 1 - \frac{\sum S_i \times h_i}{S \times H} \tag{10}$$

where V is the volume of the block, V_i is the volume of each building, h_i is the height of each building, S_i is the floor area of each building, S is the area of the block, and H is the height of the block.

Figure 1. Research block zoning.

The permeability K and Forchheimer coefficient C_F for the form drag can be calculated as follows:

$$K = \frac{\phi^3 {d_p}^2}{150(1-\phi^2)} \tag{11}$$

$$C_F = \frac{1.75}{\sqrt{150\phi^3}} \tag{12}$$

where d_p is the characteristic size of the solid particles in the porous media.

2.3. Physical Model

Model validation is the key to determine the accuracy and reliability of the numerical simulation. In urban simulations, the sensing size of the measuring instruments is too small relative to the study area. It is necessary to arrange numerous measuring points to obtain data representing the entire area, which is difficult to achieve in practice. Therefore, it is more practical to validate porous media models at the microscale. The representative high-density block buildings in the central area of Xinjiekou, Nanjing, in hot summer and cold winter areas, were selected as the research object. Streets surround the selected block, and the buildings in the block are almost always north–south orientation. According to Ma Jian's [31] simulation results of streets with different aspect ratios, when B/H = 0~1 and B/W = 0~1, the whole building group can be integrated into an integral building, as shown in Figure 2. Based on the site investigation, the simulated areas are divided into 7 building blocks with different porosities, as shown in Figure 1.

The models established by standard CFD modeling and the porous media model method are shown in Figures 3 and 4. Due to the limitation of computer power and the complexity of the research object, the local model of the building group is appropriately simplified in the standard CFD modeling. When the porous model is established, the research method proposed by Wang et al. [9] is used to perform additional processing on the block. In order to fully develop the airflow and ensure the accuracy of the calculation, the computational domain was extended by 3H in the vertical direction and by more than 5H in the other four directions (where H is the height of the highest building in the block).

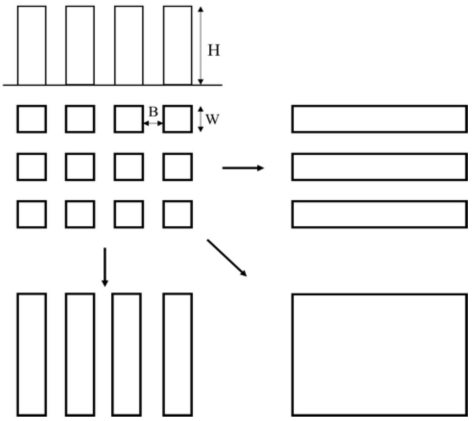

Figure 2. Modeling method of porous media.

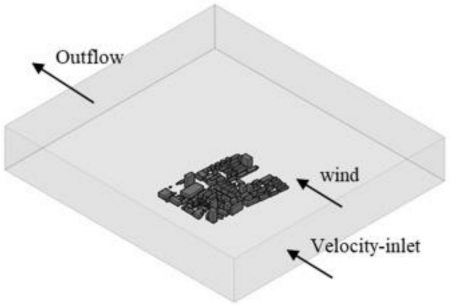

Figure 3. Modeling for the standard CFD method.

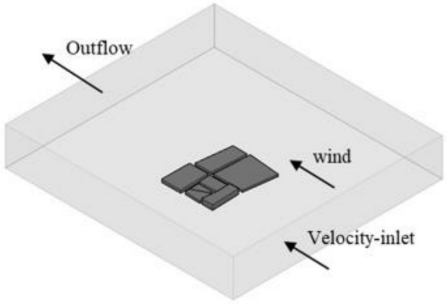

Figure 4. Method for modeling porous media.

When the standard CFD method divides the model grid, the building group was the key research object, and the grid independence test was carried out. After setting the same boundary conditions for the four grids with grid numbers of 1,789,673, 2,185,209, 3,268,935, and 4,195,998, the simulations were performed separately, and the average wind speed at the outlet of the block was recorded. The simulation results were 0.341, 0.384, 0.430, and 0.449 m/s, respectively, indicating that when the number of grids exceeds 3 million, the simulation results tend to be stable (the difference is about 4.4%). Therefore, subsequent calculations of standard CFD method would use grids with a grid number of about 3 million for calculation. The porous media model uses the same method to evaluate the meshes with the number of meshes of 797,651, 1,847,621, 2,767,710, and 3,952,174 and four meshes, namely 2,767,710. The meshes of the two models are shown in Figures 5 and 6.

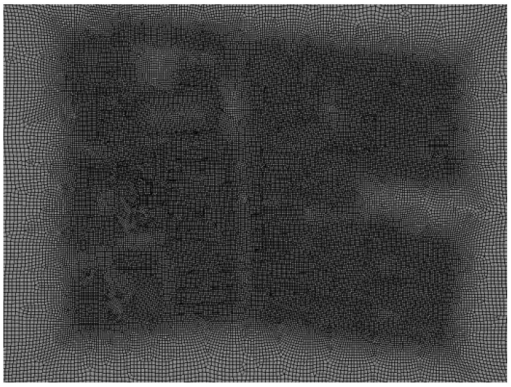

Figure 5. Mesh for the standard CFD method.

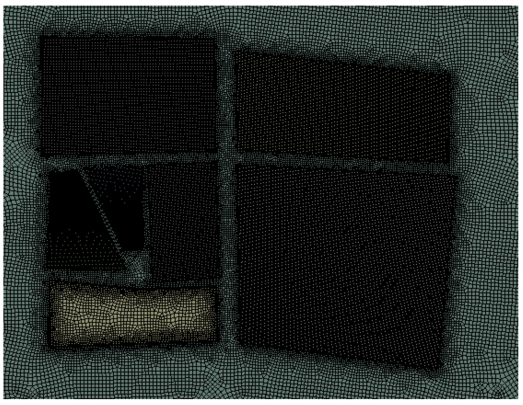

Figure 6. Mesh for modeling porous media.

2.4. Boundary Conditions and Simulation Settings

When simulating the micro-thermal environment of the block, setting reasonable boundary condition parameters can make the simulation result closer to the actual situation.

The inlet was set as the velocity inlet, and the wind speed varied with the height. For the distribution of the incoming wind speed, the most commonly used exponential law [32] was used, such as below:

$$\frac{u_{in}}{u_{zef}} = \left(\frac{z_{in}}{z_{ref}}\right)^{\alpha} \tag{13}$$

where u_{zef} is the average wind speed of incoming flow at the height of Z_{ref}; u_{in} is the average wind speed at Z_{in} at any height, α is the ground roughness coefficient, which is taken as 0.22 in the urban center according to China's specifications.

The inlet air temperature was set as 32 °C, and the wind direction was set as south. The outlet boundary was set as the outflow boundary condition.

The profiles of turbulent kinetic energy ($\kappa_{in}(z)$) and its dissipation ($\varepsilon_{in}(z)$) [7] at the domain inlet were calculated as described in Equations (14) and (15).

$$\kappa_{in}(z) = 0.01{u_{zef}}^2 \tag{14}$$

$$\varepsilon_{in}(z) = \frac{{c_\mu}^{3/4}\kappa_{in}(z)^{3/2}}{k_v z} \tag{15}$$

where $c_\mu = 0.09$, k_v is von Karman's constant, taken as 0.4.

Other boundaries, such as the top and sides of the domain, were set to symmetry boundaries. The anthropogenic heat was simplified to the heat source intensity based on the surface area for the thermal boundary conditions, and the surface heat flux was given. In order to compare the simulation results of the porous media method and the standard CFD method sufficiently, the standard CFD method and the porous media method

use the same size calculation domain and consistent boundary conditions. The boundary conditions of the model using both methods are detailed in Table 1.

Table 1. Setting of boundary conditions.

Surfaces	Standard CFD Model	Porous Media Model
Inlet	Velocity inlet	Velocity inlet
Outlet	Outflow	Outflow
Top and sides	Symmetry	Symmetry
Underlying surface	Non-slipping wall	Non-slipping wall
Building wall	Non-slipping wall	—
Porous zone	—	Interior

When simulating calculations, the standard CFD method and the porous media method use the same solution settings. The control volume method was used to discretize the equation in the simulation calculation. The RNG k–ε turbulence model is employed. The coupling relationship between velocity and pressure was the SIMPLEC scheme, and the residual was less than 10^{-5}. The convection term and the diffusion term were simulated by the second-order upwind style, which had higher accuracy and slower convergence speed. After several attempts, the under-relaxation factor for speed and pressure was set to 0.5 and the other factor below 0.5.

3. Actual Measurement Verification

3.1. Measured Plan

Model validation is the key to determining the accuracy and reliability of numerical simulations. In this study, the standard CFD modeling method and the porous media method were used to simulate the micro-thermal environment of the block, and the measurement points were measured in the block to verify the accuracy of the simulation results. In this paper, the "virtual synchronous measurement method" was selected for measurement on a typical summer day in July. The measurement points were mainly selected along the main road, the corner of the building, and the open space around the building, and the measurement height was about 1.5 m. The measuring device was used for each measurement point test time of 10 min, every interval of 30 s to record the data, the average value was taken as the result, and the instrument parameters tested are shown in Table 2. The selection of measuring points is shown in Figure 7, and the field measurement is shown in Figure 8.

Table 2. Measurement device parameters.

Name	Measuring Parameters	Range	Resolution	Precision
GM1361 split type of thermometer	Temperature	−10–50 °C	0.1 °C	±1.0 °C
Anemometer	Velocity	0~45 m/s	0.1 m/s	±0.3 m/s

3.2. Comparison of Measured and Simulated Results

The measurement results of each measuring point in the block were obtained from the above measurement method, and the average values were calculated respectively. The results show that the wind speed changes violently at each time in a short time, while the temperature changes relatively gently, so the temperature standard deviation is of more research significance. The results are shown in Table 3.

Figure 7. The field measurement points.

Figure 8. Photo of field measurement.

Table 3. Measurement results and standard deviation of temperature.

Parameters	Velocity (m/s)	Temperature (K)	Standard Deviation of Temperature
1	0.284	310.1	0.116
2	0.345	309.4	0.136
3	0.39	309.2	0.196
4	0.317	308.7	0.129
5	0.26	308.1	0.143
6	0.22	309.6	0.123
7	0.396	309.1	0.219
8	0.54	308.8	0.224

Since the monitoring points in the simulation may be different from the field measurement points, the average values of 5~6 points near the simulation's monitoring points were used to compare the simulated values and the measured values. Figure 9 shows the comparison results of wind velocity and temperature between measured and simulated values at different points.

The comparison results show that the measured results using the selected measurement points are in agreement with the simulation results of both the standard CFD model and the porous media model to a high degree.

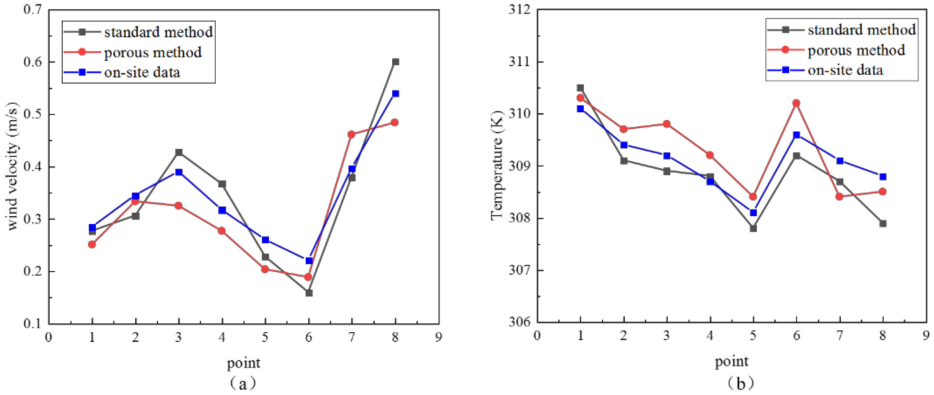

Figure 9. Comparison of measured and simulated (**a**) wind velocity and (**b**) temperature at different points.

In order to further judge the degree of agreement between the simulation results and the measured values, the coefficient of determination R^2 was used to measure the degree of fitting between the simulation results and the measured values. The closer R^2 is to 1, the better the fitting is. The calculation formula is as follows:

$$R^2 = \frac{\left[\sum_i (y_i - \overline{y})(\hat{y}_i - \overline{\hat{y}})\right]^2}{\left[\sum_i (y_i - \overline{y})^2\right]\left[\sum_i (\hat{y}_i - \overline{\hat{y}})^2\right]} \tag{16}$$

The R^2 for each of the two methods is shown in the Table 4.

Table 4. Coefficient of determination.

Simulation Method	Velocity	Temperature
Porous media method	0.86	0.67
Standard CFD simulation method	0.94	0.83

The R^2 values of wind velocity and temperature between the standard CFD simulation method and the porous media simulation are 0.08 and 0.16, respectively. It is indicated that the accuracy of the standard CFD simulation method is slightly higher in comparison. Nevertheless, the R^2 obtained by either the standard CFD method simulation or the porous media model method is above 0.65, which indicates that the fitting effect is better and both methods can effectively reflect the thermal environment of the block.

4. Discussion

4.1. Comparison between Porous Media Modeling Method and Standard Modeling Method

4.1.1. Comparative Analysis of Calculation Results

The simulation results of the standard model and the porous media model are compared to analyze further the feasibility of using the porous media modeling method instead of the standard CFD modeling method in studying the microthermal environment of the block. Figure 10 shows the wind velocity at the pedestrian height of the block using two methods, respectively, and Figure 11 shows the cloud diagram of temperature distribution. The velocity and temperature distribution in the block are similar to different simulation methods, and the porous media model method can characterize the micro-thermal environment of each block zone well. In the main road between buildings, especially in the south–north direction of the main street, the wind speed shows a trend of attenuation along the direction of the street, which promotes ventilation to improve the micro-thermal environment of the block. The velocity of the main street calculated by both methods is between 0.5 and 0.62 m/s, and the temperature is between 307 and 309 K.

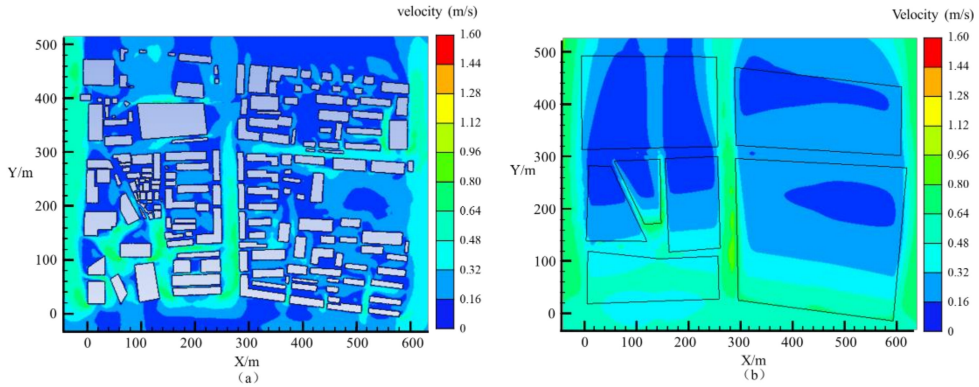

Figure 10. Diagram of wind velocity distribution modeled by the (**a**) standard CFD method and (**b**) porous media method.

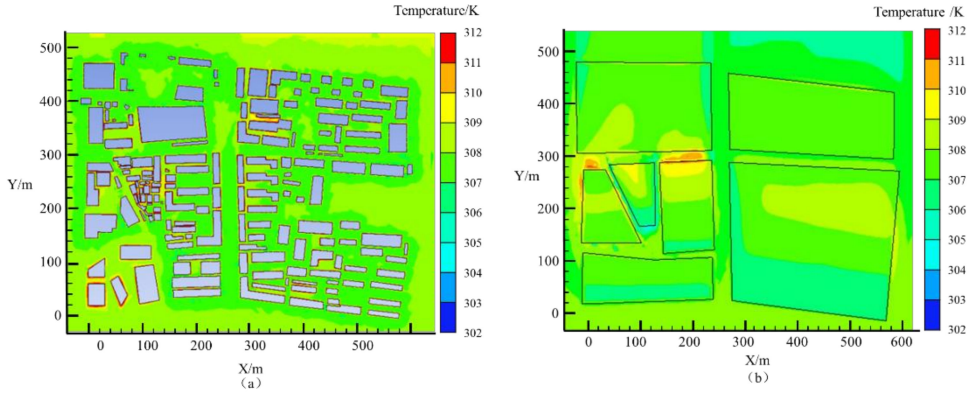

Figure 11. Diagram of temperature distribution modeled by the (**a**) standard CFD method and (**b**) porous media method.

Because the porous media method simplifies the geometric shape of the actual building, the overall thermal environment characteristics of the region are more conducive to comparison and verification than the interior points of the building cluster. According to the simulation results, each region's average wind velocity and temperature are calculated, respectively, and the results are shown in Figure 12. The distribution trends of wind speed and temperature in different regions are the same. The maximum value of wind speed and the minimum value of temperature are obtained in area 6, and the minimum value of wind velocity and the maximum value of temperature are obtained in area 4. The maximum variation in wind velocity between the regions using the standard CFD model and the porous media model is 0.51 and 0.60 m/s, respectively, and the maximum variation in temperature is 1.6 and 1.2 K. The maximum variation in average wind speed of each region obtained by different methods is only 0.07 m/s, the maximum variation in temperature is 1.4 K, and the maximum error is less than 10%. Thus, it can be seen that the mean temperature and wind velocity of each region are in good agreement with each other.

Comparing the overall characteristics of the microenvironment within each zoning area and along the central axis when the microthermal environment was modeled using both standard CFD and porous media methods, it was observed that the wind velocity distributions and temperature distributions were similar between the standard CFD modeling approach and the porous media approach. Additionally, porous media are effective in reflecting the wind and thermal environments of the building complex as a whole and of the nearby main street.

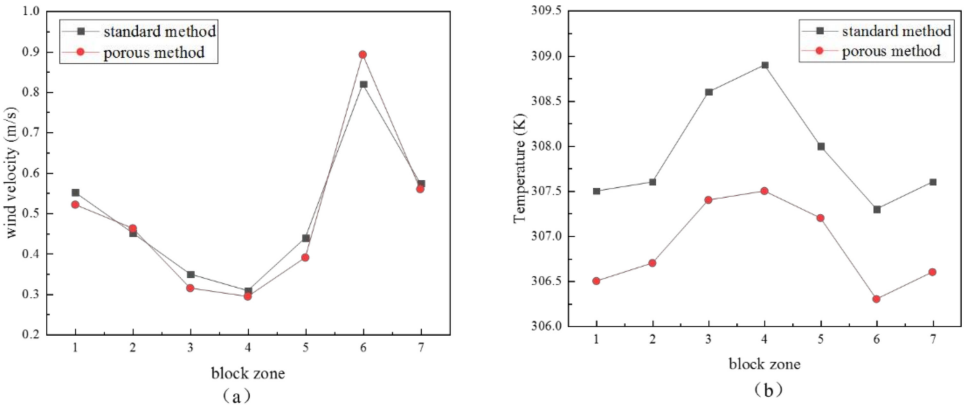

Figure 12. (**a**) Mean wind velocity and (**b**) mean temperature in different block zones.

4.1.2. Comparative Analysis of Computational Cost

When the computer with the same performance was used for simulation, the two simulation methods' running time and iterative step size are shown in Table 5. The results show that the porous media model method reduces the number of grids by about 15.3% compared with the standard method. The porous media model method takes only 6 s to complete one iteration, while the standard method requires 14.2 s. The porous media model method and the standard method converge after 854 and 1516 steps, respectively, and the total number of iterations of the porous media model method is reduced by 43.6%. The standard CFD method takes about 480 min to achieve convergence, while the porous media model method takes only about 140 min, about 70.8% faster than the standard method. Compared with the standard CFD modeling method, the porous media model method has the advantages of simple implementation, low cost of computing resources, and can effectively simulate the overall micro-thermal environment of the block. Therefore, the porous media method can reduce the computational cost of microclimate research and practice and is of great value in the initial micro-environmental assessment.

Table 5. Simulation cost comparison.

	Standard CFD Modeling Method	**Porous Media Model Method**
Number of grids	3,268,935	2,767,710
Time per iteration/s	14~20	6~12
Number of iterations	1516	854
Simulation time/min	480	140

When designing a comprehensive city, the two methods must be combined or alternated according to the type of project and its requirements. A porous media model should be used for determining the main comprehensive partitions and ventilation corridors, whereas a standard model should be used for determining the surrounding areas of important structures. Consequently, the problems associated with the standard methods taking a long time to simulate as well as those associated with the porous media model not being able to accurately reflect the micro-thermal environment within a specific building can be simultaneously solved.

4.2. Effect of Porous Media Parameters on Micro-Thermal Environment

When it comes to porous media blocks, porosity indicates the density of the building layout within the block, and its size has an important influence on the ventilation capacity of the block. In order to explore the influence of porosity on the microthermal environment of the actual block, the zones with different porosity, except zones 6 and 1, where the average building height is much higher than that of the other zones, were selected to study the corresponding wind velocity and temperature at the heights of 2, 10, and 50 m (Figure 13).

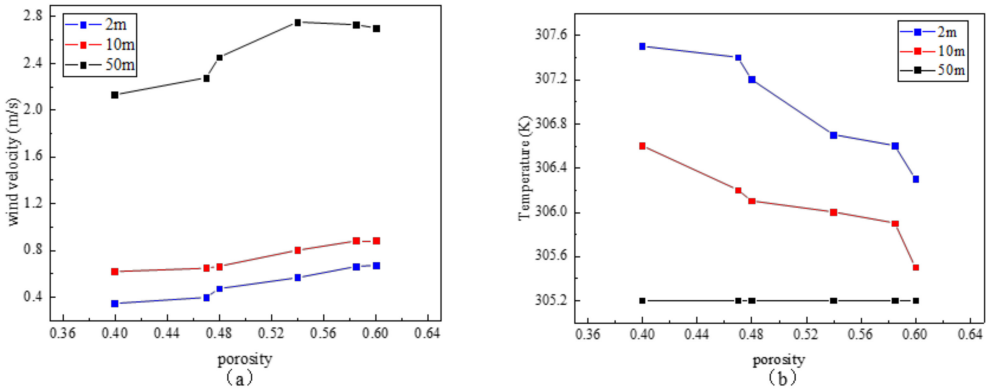

Figure 13. Effect of porosity on (**a**) wind velocity and (**b**) temperature at different heights.

The results show a positive correlation between wind velocity and porosity at different heights and a negative correlation between temperature and porosity. The greater the porosity in the dominant wind direction, the higher the average wind velocity, and the better the ventilation environment of the block. At the height of 2 m, the change in wind speed and porosity in each zone is the most obvious. The wind velocity in the area with porosity of 0.6 is about 0.32 m/s higher than that in the area with porosity of 0.4, and the temperature is about 0.9 K lower. The wind velocity in different porosity zones at 10 m height is about 0.25 m/s higher than that at 2 m height, and the temperature is about 0.9 K lower, but the variation law of wind velocity and temperature is basically the same as that at 2 m height. As the wind velocity at the block entrance changes exponentially with height, the higher the height, the greater the wind velocity, and the higher wind velocity can quickly transport and diffuse the heat. The wind velocity at 50 m height will still be affected by the airflow disturbance on the edge of the block, but the temperature hardly changes with porosity change.

4.3. Influence of Anthropogenic Heat on Micro-Thermal Environment

Based on Luo et al.'s [33,34] research on urban anthropogenic heat emission, four anthropogenic heat intensities with values of 0, 20, 40, and 60 W/m^2 were selected in this study to investigate the effects of anthropogenic heat intensity on the microthermal environment of the block. They represent non-anthropogenic heat emission, anthropogenic heat intensity in other cities, anthropogenic heat intensity in the study area, and anthropogenic heat intensity in the central city of Nanjing, respectively. Figure 14 shows the effect of anthropogenic heat on the block at different heights.

The results show that the mean temperature of each area at different heights increases significantly with the increase in the anthropogenic heat intensity in the block. Furthermore, since the anthropogenic heat will diffuse downstream with the wind direction, the upstream heat source intensity will impact the downstream streets and areas, which is the main reason for the significantly higher temperature in Block 1. The distribution of wind speed and temperature in each area is also in line with the law that the block with high porosity has high wind speed and low temperature. When the airflow enters the block, the wind velocity in the area with large porosity is relatively large, and the high-speed wind increases the heat. The exchange flux makes the anthropogenic heat dissipate rapidly, so the anthropogenic heat has relatively little effect on the areas with high porosity. At the heights of 2 and 10 m, the temperature distribution in each region is basically the same. At the height of 2 m, the variation gradient of anthropogenic heat is about 0.025 K/W. However, at the height of 10 m, due to the increase in wind speed and the effect of lateral wind, the heat diffuses relatively faster, and the influence of anthropogenic heat on the thermal environment at this height is weakened. Since the average building height is lower than 50 m, the anthropogenic heat intensity at the height of 50 m has little effect on the thermal environment.

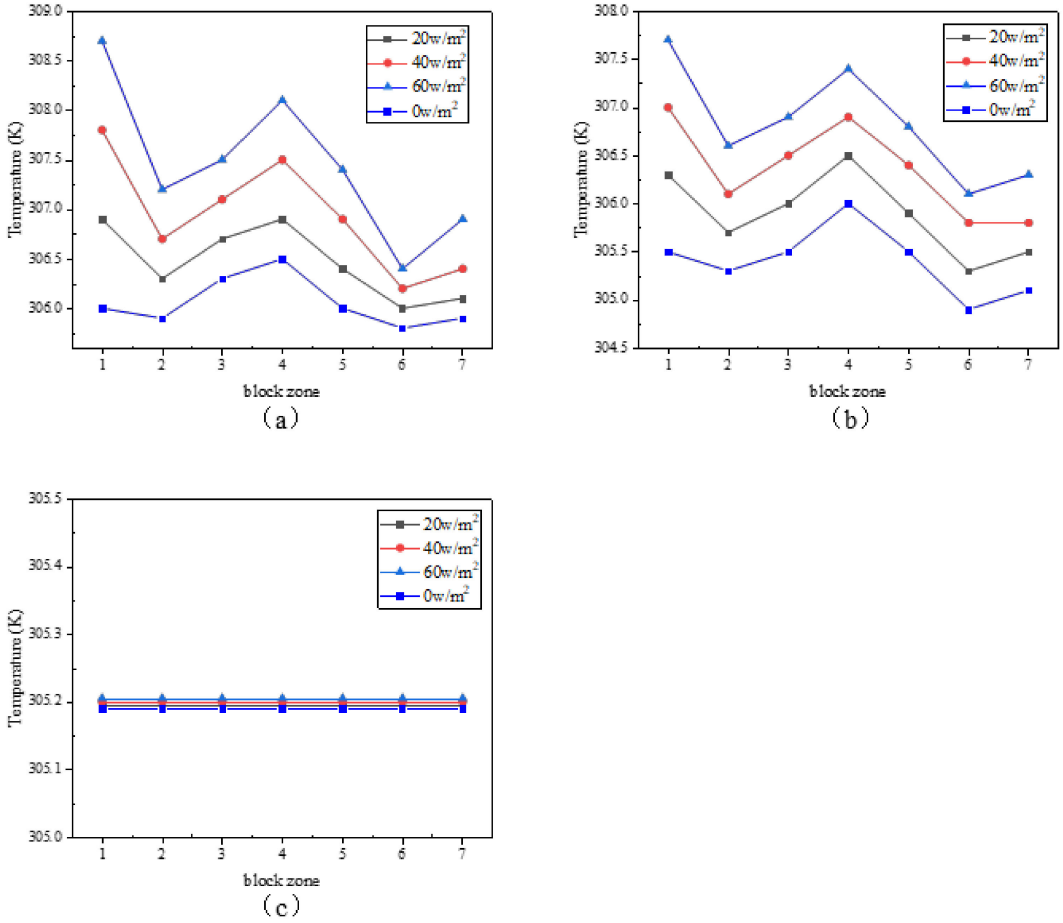

Figure 14. Temperature of the area corresponding to the heights of 2 m (**a**), 10 m (**b**), and 50 m (**c**) under different intensities of anthropogenic heat.

Accordingly, the intensity of anthropogenic heat emission plays a crucial role in the formation of the microthermal environment of the block. In order to alleviate the urban heat island effect in summer, the first consideration should be given to reducing the intensity of urban anthropogenic heat emission. Although the anthropogenic heat intensity has almost no effect on the wind velocity of the block, the wind velocity determines the speed of heat diffusion. The more significant wind velocity allows for rapid transport of heat generated by the block. Various methods, such as changing the layout and increasing the porosity of the block, can be used to promote airflow and improve the microthermal environment of the block.

5. Conclusions

In this paper, the standard CFD modeling and porous media method simulation were verified by actual measurement and comparison. The influence of porous media parameters and anthropogenic heat intensity on the thermal environment of the block was analyzed. The main findings can be summarized as follows:

(1) The actual measurement shows that both the porous media method and the standard model method can accurately characterize the overall regional ventilation capacity of the building complex. The wind speed and temperature of each area in the block with different simulation methods have a similar distribution. Porous media also improves the efficiency of modeling and calculation. The porous media model method reduces the number of meshes by about 15.3% compared with the traditional method, and the calculation rate is about 70.8% faster than the traditional method.

(2) As an essential parameter of porous media, porosity, reflects the density of the building layout in the block. From the building ground to the average height of the block, the wind speed is positively correlated with the porosity change, and the temperature is negatively correlated with the porosity change. Above the block height, say 50 m, the wind speed is still affected by the porosity due to airflow disturbances over the block edge, but the temperature is hardly affected by the porosity at this height.
(3) The anthropogenic heat emission is one of the critical factors leading to increased temperature in the block. The intensity of anthropogenic heat has little effect on the wind speed of the block, but the regional temperature at the same height increases linearly with the intensity of anthropogenic heat. The change gradient is about 0.025 K/W.

Accordingly, the porous media method can save a lot of time and cost required for research on microthermal environments compared with the standard CFD modeling calculation. Using this method can significantly reduce the time and workload of urban planners for numerical simulation of microclimates and provide a particular reference value for comprehensive urban design and planning based on climate improvement. At the same time, increasing the porosity of the block and controlling the intensity of anthropogenic heat emission can improve the micro-thermal environment from two crucial aspects: enhancing ventilation and reducing heat gain, which is of great significance for alleviating the heat island effect. Since the practical application of the porous media method is still in its early stages, in the future, parameterizing the porous media as a function of horizontal or vertical changes may be considered to address the challenges posed by uneven building heights and inaccuracies caused by complex building environments.

Author Contributions: Conceptualization, Z.C. and J.L.; methodology, J.L.; software, J.L.; validation, D.W. and J.L.; formal analysis, D.W. and J.L.; investigation, D.W. and J.L.; resources, D.W. and J.L.; data curation, D.W. and J.L.; writing—original draft preparation, J.L.; writing—review and editing, Z.C. and J.L.; visualization, J.L.; supervision, Z.C. and J.L.; project administration, Z.C.; funding acquisition, Z.C. All authors have read and agreed to the published version of the manuscript.

Funding: This research was funded by The Renewable Energy Multi-Energy Complementary Heating Key Technology Research and Demonstration, the funding number is 2021ZD26.

Data Availability Statement: Not applicable.

Acknowledgments: The author wishes to express his appreciation and gratitude to the anonymous reviewers and editors for their insightful comments and suggestions to improve the paper's quality.

Conflicts of Interest: The authors declare no conflict of interest.

Nomenclature

u_i^f	intrinsic averages of time-averaged velocity components ($m \cdot s^{-1}$)
x_i	Cartesian coordinates
T	temperature (°C)
p^f	intrinsic averages of time-averaged pressure (Pa)
k^f	intrinsic averages of time-averaged turbulent kinetic energy ($m^2 \cdot s^{-2}$)
J_1	viscosity ratio
k	von Karman's constant, 0.4
Q^f	intrinsic averages of time-averaged velocity ($m \cdot s^{-1}$)
C_μ	constant value: 0.09
K	permeability (m^2)
C_F	Forchheimer coefficient
d_p	characteristic size of the solid particles (m)

U	volume of the porous media (m^3)
V	volume of the block (m^3)
h_i	height of each building (m)
S_i	floor area of each building (m^2)
S	area of the block (m^2)
H	height of the block (m)
u	average wind speed (m/s)
z	height (m)
R^2	coefficient of determination
y_i	measured value
$\overline{y}$	mean measured value
$\hat{y}_i$	simulation value
Greek symbols	
ϕ	porosity
ρ	density ($kg \cdot m^{-3}$)
β	thermal expansion coefficient (K^{-1})
μ_l	dynamic viscosities ($kg \cdot m^{-1} \cdot s^{-2}$)
μ_t	turbulent viscosities ($kg \cdot m^{-1} \cdot s^{-2}$)
δ_{ij}	Kronecker delta operator
ε^f	intrinsic averages of time-averaged dissipation ($m^2 \cdot s^{-3}$)
α	ground roughness coefficient
k	turbulent kinetic energy ($m^2 \cdot s^{-2}$)
ε	dissipation of k ($m^2 \cdot s^{-3}$)
ϕ	porosity
Subscripts	
in	inlet
ref	reference

References

1. Zhong, S.; Qian, Y.; Zhao, C.; Leung, R.; Yang, X.Q. A case study of urbanization impact on summer precipitation in the greater Beijing metropolitan area: Urban heat island versus aerosol effects. *J. Geophys. Res.-Atmos.* **2015**, *120*, 10903–10914. [CrossRef]
2. Toparlar, Y.; Blocken, B.; Maiheu, B.; Van Heijst, G.J.F. A review on the CFD analysis of urban microclimate. *Renew. Sustain. Energy Rev.* **2017**, *80*, 1613–1640. [CrossRef]
3. Ashie, Y.; Kono, T. Urban-scale CFD analysis in support of a climate-sensitive design for the Tokyo Bay area. *Int. J. Climatol.* **2011**, *31*, 174–188. [CrossRef]
4. Mahgoub, A.O.; Ghani, S. Numerical and experimental investigation of utilizing the porous media model for windbreaks CFD simulation. *Sustain. Cities Soc.* **2021**, *65*, 102648. [CrossRef]
5. Skote, M.; Sandberg, M.; Westerberg, U.; Claesson, L.; Johansson, A.V. Numerical and experimental studies of wind environment in an urban morphology. *Atmos. Environ.* **2005**, *39*, 6147–6158. [CrossRef]
6. Antohe, B.V.; Lage, J.L. A general two-equation macroscopic turbulence model for incompressible flow in porous media. *Int. J. Heat Mass Transf.* **1997**, *40*, 3013–3024. [CrossRef]
7. Hang, J.; Li, Y. Wind conditions in idealized building clusters: Macroscopic simulations using a porous turbulence model. *Bound. Layer Meteorol.* **2010**, *136*, 129–159. [CrossRef]
8. Gu, Z.; Zhang, Y. *Large Eddy Simulation of Urban and Building Wind Environment and Application*; Science Press: Beijing, China, 2014. (In Chinese)
9. Wang, X.; Li, Y.; Hang, J. A combined fully-resolved and porous approach for building cluster wind flows. *Build. Simul.* **2017**, *10*, 97–109. [CrossRef]
10. Tiantian, L.; Bingfeng, Y.; Zhangbao, H.; Zhi, C. Numerical Simulation on Impact of Building Density on Urban Heat Island with an Urban Porous Media Model. *J. Xi'an Jiaotong Univ.* **2012**, *46*, 134–138.
11. Ming, T.; Lian, S.; Wu, Y.; Shi, T.; Peng, C.; Fang, Y.; de Richter, R.; Wong, N.H. Numerical investigation on the urban heat island effect by using a porous media model. *Energies* **2021**, *14*, 4681. [CrossRef]
12. Sun, R.; Wang, Y.; Chen, T. Impacts of anthropogenic heat emissions on urban thermal environment: A review. *Acta Ecol. Sin.* **2017**, *37*, 3991–3997. (In Chinese)
13. Kim, G.; Cha, D.H.; Song, C.K.; Kim, H. Impacts of Anthropogenic Heat and Building Height on Urban Precipitation Over the Seoul Metropolitan area in Regional Climate Modeling. *J. Geophys. Res.-Atmos.* **2021**, *126*, e2021JD035348. [CrossRef]
14. Fung, K.Y.; Tam, C.Y.; Lee, T.C.; Wang, Z. Comparing the Influence of Global Warming and Urban Anthropogenic Heat on Extreme Precipitation in Urbanized Pearl River Delta Area Based on Dynamical Downscaling. *J. Geophys. Res.-Atmos.* **2021**, *126*, e2021JD035047. [CrossRef]

15. Falasca, S.; Catalano, F.; Moroni, M. Numerical Study of the Daytime Planetary Boundary Layer over an Idealized Urban Area: Influence of Surface Properties, Anthropogenic Heat Flux, and Geostrophic Wind Intensity. *J. Appl. Meteorol. Climatol.* **2016**, *55*, 1021–1039. [CrossRef]
16. Holst, C.C.; Tam, C.; Chan, J.C.L. Sensitivity of urban rainfall to anthropogenic heat flux: A numerical experiment. *Geophys. Res. Lett.* **2016**, *43*, 2240–2248. [CrossRef]
17. Wen, Y.; Lian, Z. Influence of air conditioners utilization on urban thermal environment. *Appl. Therm. Eng.* **2009**, *29*, 670–675. [CrossRef]
18. Quah, A.K.L.; Roth, M. Diurnal and weekly variation of anthropogenic heat emissions in a tropical city, Singapore. *Atmos. Environ.* **2012**, *46*, 92–103. [CrossRef]
19. Flanner, M.G. Integrating anthropogenic heat flux with global climate models. *Geophysical Research Letters* **2009**, 36. [CrossRef]
20. Liu, P.; Li, L.P.; Liao, J.B.; Guo, X.M.; Zhang, Y.R. A study of the effect of anthropogenic heat on meteorological factors in the summer of Shanghai City. *J. Lanzhou Univ. (Nat. Sci.)* **2019**, *55*, 267–273. (In Chinese)
21. Du, H.; Wang, D.; Wang, Y.; Zhao, X.; Qin, F.; Jiang, H.; Cai, Y. Influences of land cover types, meteorological conditions, anthropogenic heat and urban area on surface urban heat island in the Yangtze River Delta Urban Agglomeration. *Sci. Total Environ.* **2016**, *571*, 461–470. [CrossRef]
22. Xie, M.; Zhu, K.; Wang, T.; Feng, W.; Zhu, X.; Chen, F.; Ouyang, Y.; Liu, Z. Study on the distribution of anthropogenic heat flux over China. *China Environ. Sci.* **2015**, *35*, 728–734. (In Chinese)
23. Lu, Y.; Wang, Q.G.; Zhai, Y.R.; Song, Y.Y.; Zhang, Y.Y.; Sun, P. Anthropogenic heat emissions in the Yangtze River Delta region. *China Environ. Sci.* **2014**, *34*, 295–301. (In Chinese)
24. Takane, Y.; Kikegawa, Y.; Hara, M.; Grimmond, C.S.B. Urban warming and future air-conditioning use in an Asian megacity: Importance of positive feedback. *NPJ Clim. Atmos. Sci.* **2019**, *2*, 39. [CrossRef]
25. Ohashi, Y.; Suido, M.; Kikegawa, Y.; Ihara, T.; Shigeta, Y.; Nabeshima, M. Impact of seasonal variations in weekday electricity use on urban air temperature observed in Osaka, Japan. *Q. J. R. Meteorol. Soc.* **2016**, *142*, 971–982. [CrossRef]
26. Tong, H.; Liu, H.Z.; Sang, J.G.; Hu, F. The Impact of Urban Anthropogenic Heat on Beijing Heat Environment. *Clim. Environ. Res.* **2004**, *9*, 409–421. (In Chinese)
27. Jiang, W.; Chen, Y. The Impact of Anthropogenic Heat on Urban Boundary Layer Structure. *Chin. J. Atmos. Sci.* **2007**, *31*, 37–47. (In Chinese)
28. Mei, S.; Yuan, C. Analytical and numerical study on transient urban street air warming induced by anthropogenic heat emission. *Energy Build.* **2021**, *231*, 110613. [CrossRef]
29. Cao, Z.; Wen, Y.; Song, S.; Hung, C.H.; Sun, H. Spatiotemporal Variations and Controls on Anthropogenic Heat Fluxes in 12 Selected Cities in the Eastern China. *Chin. Geogr. Sci.* **2021**, *31*, 444–458. [CrossRef]
30. Yuan, C.; Adelia, A.S.; Mei, S.; He, W.; Li, X.X.; Norford, L. Mitigating intensity of urban heat island by better understanding on urban morphology and anthropogenic heat dispersion. *Build. Environ.* **2020**, *176*, 106876. [CrossRef]
31. Ma, J. *Numerical Study of Wind Environment around Building Complexes*; Zhejiang University: Zhejiang, China, 2006. (In Chinese)
32. Leung, K.K.; Liu, C.; Wong, C.C.C.; Lo, J.C.; Ng, G.C. On the study of ventilation and pollutant removal over idealized two-dimensional urban street canyons. *Build. Simul.* **2012**, *5*, 359–369. [CrossRef]
33. Luo, Y.H.; Zhu, S.Y.; Zhang, G.X.; Liu, Y.; Xiang, J.M.; Zhou, Y. Estimation and Analysis of Spatial Distribution of Urban Population During the Daytime and Nighttime in Qinhuai District of Nanjing. *Resour. Environ. Yangtze Basin* **2018**, *27*, 1020–1030. (In Chinese)
34. Yang, H.L. *Estimation on Temporal—Spatial Characteristics of Anthropogenic Heat in Qinhuai District of Nanjing Based on the Inventory Survey Method*; Nanjing University of Information Science and Technology: Nanjing, China, 2018.